Journal of Materials Science: Materials in Electronics (2019) 30:6811–6819
https://doi.org/10.1007/s10854-019-00993-y

Fabrication of *p*-NiO nanoflakes/*n*-Si(100) heterojunction architecture for high sensitive photodetectors

G. Jayalakshmi[1] · K. Saravanan[1] · J. Navas[1] · T. Arun[2] · B. K. Panigrahi[3]

Received: 28 November 2018 / Accepted: 21 February 2019 / Published online: 26 February 2019

Abstract
We report the facile hydrothermal synthesis of *p*-NiO nanoflakes (NFs)/*n*-Si (100) heterojunction architecture and its photoresponse behavior. The vertically grown NiO NFs architecture is clearly seen on the Si substrate, as evidenced from the field emission scanning electron microscopy images. The elemental composition of the grown nanostructure on the Si substrate was estimated using energy-dispersive X-ray spectroscopy, and resonant Rutherford backscattering spectrometry measurements. The grazing incidence X-ray diffraction measurement reveals the grown NiO NFs architecture is of face centered cubic phase. The I-V characteristics of *p*-NiO NFs/*n*-Si heterojunction architecture shows good rectifying behavior in the dark and the increased photocurrent in the reverse bias imply the formation of *p*–*n* junction at the interface of *p*-NiO NFs and *n*-Si substrate. The voltage-dependent sensitivity of the device reveals the highest sensitivity at reverse bias of 3 V. The time-dependent photoresponse measurements of the device show good stability and repeatability under blue light illumination. The response and recovery time of the device is found as 6.18 s and 1.83 s under the reverse bias of 3 V. Our experimental studies demonstrate that the fabricated *p*-NiO NFs/*n*-Si heterojunction device has considerable promise for the practical photodetector applications.

1 Introduction

In recent years, low-dimensional nanostructured materials have attracted wide-spread attention for the fabrication of novel optoelectronic and sensing devices due to its large surface-to-volume ratio, good electrical conductivity, high carrier mobility, high optical transparency and tunable optical properties [1–5]. In particular, the development of efficient photodetectors is of current interest due to its potential applications in image sensing, missile tracking, flame detection, and optical communications etc [6, 7]. In this regard, two dimensional (2D) wide bandgap nanostructured materials such as ZnO, TiO_2, GaN, SiC, NiO have been considered as the excellent candidates for the fabrication of efficient photodetectors [7–11]. Among them, NiO is a *p*-type semiconductor with a band gap in the range of 3.6–4.0 eV, has received considerable interest due to its excellent electronic, optical and electrochemical properties desirable for making the smart windows, cathodes for the dye-sensitized solar cells, electrochemical capacitors, gas sensors, electrochemical devices, field emission displays and optoelectronic devices etc [12–14]. In addition, NiO has strong absorption in the UV-blue region owing to its *d*–*d* band transitions and found that its resistivity depends on the concentration of the cation (Ni) vacancies suggesting NiO is a promising candidate for the photodetector based applications [15].

To develop high efficient photodetectors, several strategies have been employed such as the fabrication of *p*–*n* homojunctions, *p*–*n* heterojunctions, Schottky junctions, and metal-semiconductor-metal photodetectors [12, 16–19]. The fabrication of *p*–*n* heterojunction photodetector based on NiO nanostructures on the Si substrate is an effective way for obtaining the UV-blue photodetectors due to the strong electric field built at the interface between NiO and Si reduces the leakage current, which in turn improves the photocurrent, as well as recovery speed. Until, recently *p*-NiO/*n*-Si heterojunction photodetectors have also been reported for the UV and visible photodetection [12, 20, 21]. Zhang et al. have fabricated NiO/

✉ G. Jayalakshmi
jayasrnmc@gmail.com

[1] Materials Science Group, Indira Gandhi Centre for Atomic Research, Kalpakkam, Tamil Nadu 603102, India

[2] Institute of Physics, Bhubaneswar, Odisha 751005, India

[3] Electronics and Instrumentation Group, Indira Gandhi Centre for Atomic Research, HBNI, Kalpakkam, Tamil Nadu 603102, India

Si heterojunction diodes by UV oxidation of metallic Ni deposited on the *n*-Si substrate and observed that NiO/*n*-Si heterojunction shows the rectification of two orders of magnitude higher than NiO/*p*-Si heterojunction for the voltage sweep − 2 V to + 2 V [21]. Parida et al. have reported the photoresponse behavior of NiO/*n*-Si heterojunction photodetector by using spin coating of colloidal $Ni(OH)_2$, subsequently annealed at 400 °C in air ambient and observed photocurrent of 0.125, 0.21 and 0.27 µA for UV, green and red light sources of power densities 1.1, 0.69 and 0.22 mW/cm^2, respectively [12]. However, it is reported that the fabricated NiO/Si heterojunction photodetectors have also been severely suffered by the large leakage current due to the diffusion of Ni into the Si substrate due to the high-temperature deposition techniques adopted for the fabrication process [11, 20, 21]. To overcome these issues, we have adopted a facile hydrothermal technique for the synthesis of NiO nanoflakes (NFs) architecture on the Si (100) substrate, as it is simple, low cost, large scale production, shape and the dimension of the NiO nanostructures can be controlled by the growth parameters. The current–voltage (I–V) characteristics and photoresponse performance of *p*-NiO NFs/*n*-Si heterojunction architecture was investigated, and the mechanism on blue light detection has also been discussed in detail.

2 Experimental details

Figure 1a, b illustrates the schematic synthesis process of NiO NFs architecture grown on Si substrate and the fabricated *p*-NiO NFs/*n*-Si heterojunction photodetector. The detailed synthesis procedure is given in our earlier report [14]. Briefly, NiO NFs architecture was grown on the Si substrate by a facile hydrothermal synthesis route. Prior to the deposition of NiO NFs architecture, Ni seed layer was deposited on ultrasonically cleaned Si substrate using pulsed laser deposition technique. For the growth of NiO NFs architecture, Ni seeded Si substrate was kept face down in the equimolar (0.1 M) aqueous solution of Nickel (II) nitrate hexahydrate ($Ni(NO_3)_2.6H_2O$) and hexamethylenetetramine (HMTA) mixture, and then mixture was heated constantly at 95 °C for four hours. The substrate was then taken out from the growth solution, and rinsed with the deionized water many times, and then annealed at 600 °C in air ambient for 1 h. Finally, *p*-NiO NFs/*n*-Si heterojunction photodetector was fabricated by taking the Ag electrodes on *p*-NiO NFs architecture and the underlying Si substrate as schematically shown in the Fig. 1b.

The surface morphology of the grown sample was investigated using field emission scanning electron microscope (FESEM; Carl Zeiss-Neon 40). The elemental composition of the sample was analyzed by energy-dispersive

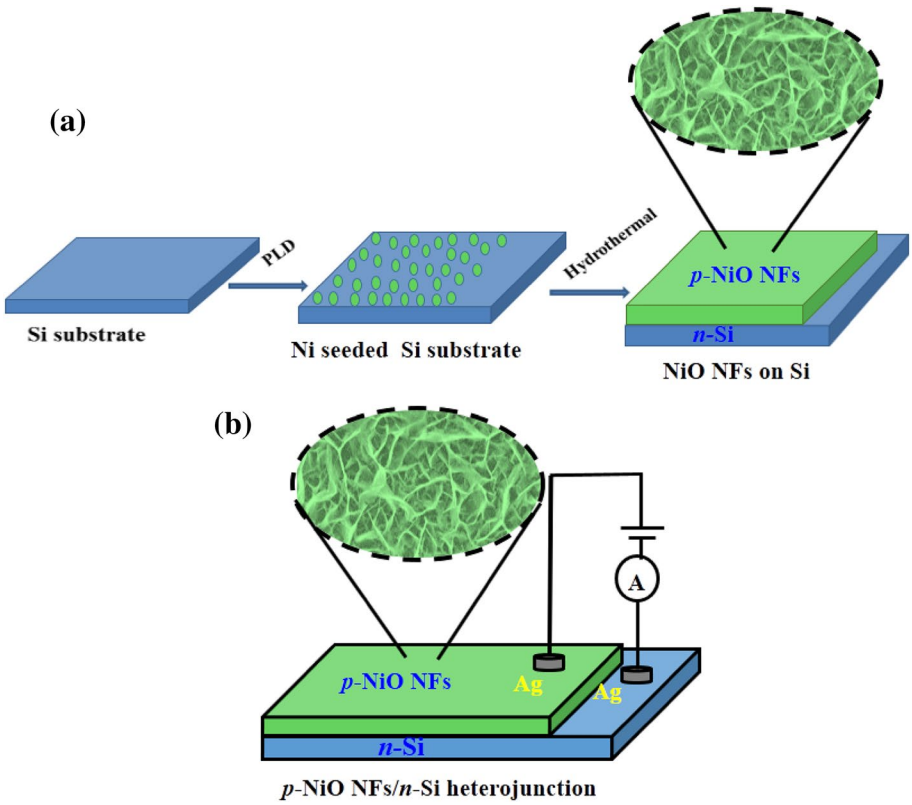

Fig. 1 **a** The schematic illustration of synthesis process of NiO NFs architecture grown on the Si substrate and **b** the fabricated *p*-NiO NFs/*n*-Si heterojunction photodetector

X-ray spectroscopy using an EDX detector (INCA, Oxford) and the resonant Rutherford backscattering spectrometry (RRBS) measurements using the 3.045 MeV He^{++} particles from 1.7 MV Tandetron accelerator (HVEE, The Netherlands). The crystalline structure of the grown sample was investigated using Inel Equinox 2000 X-ray diffractometer operating at 40 kV, 30 mA with Cu K_α radiation of wavelength, 1.5406 Å by the grazing incidence method. Raman and photoluminescence measurement of the sample was recorded using WITech Alpha300 RA spectrometer with the excitation wavelength of 532 and 355 nm, respectively in the backscattering geometry. The current–voltage (I–V) characteristics of the *p*-NiO NFs/*n*-Si heterojunction photodetector was performed using Hewlett Packard 34401A multimeter and Keithley 6517A Electrometer/High Resistance Meter with the voltage sweeps from − 5 V to + 5 V. The time-dependent photoresponse measurements were performed in the dark and illumination with the blue LED of wavelength, 450 nm and power of ~ 2.5 mW at different bias voltage ranging from to – 1 to − 3 V.

3 Results and discussion

Surface morphology and elemental composition of NiO NFs architecture was examined using FE-SEM and EDX analyses and is presented in Fig. 2. The low and high magnification images of NiO NFs architecture shown in Figs. 1b and 2a exhibits vertically aligned, densely packed, well interconnected NFs forming a network on the Si substrate. EDX spectra of NiO NFs architecture on the Si substrate is shown in Fig. 2c. The inset of Fig. 2c shows the compositions profile of the elements present in the grown nanostructure. EDX spectrum of NiO NFs architecture clearly reveals the presence of Ni, O and Si elements. The enlarged peak observed at about 1.8 keV is attributed to the Si peak emerged from the substrate. The prominent peaks observed at about 0.6 keV, 0.85 keV, 7.45 keV and 8.25 keV, are attributed to the O–*K*, Ni–$L_{\beta 1}$, Ni–$K_{\beta 1}$, and Ni–$K_{\alpha 1}$ shells, respectively [22]. Besides the nickel, oxygen, and Si, no other elements were observed, indicating the high purity of the grown nanostructure.

The elemental composition and thickness of *p*-NiO NFs/*n*-Si heterojunction architecture was performed by RRBS measurement using the oxygen resonant energy

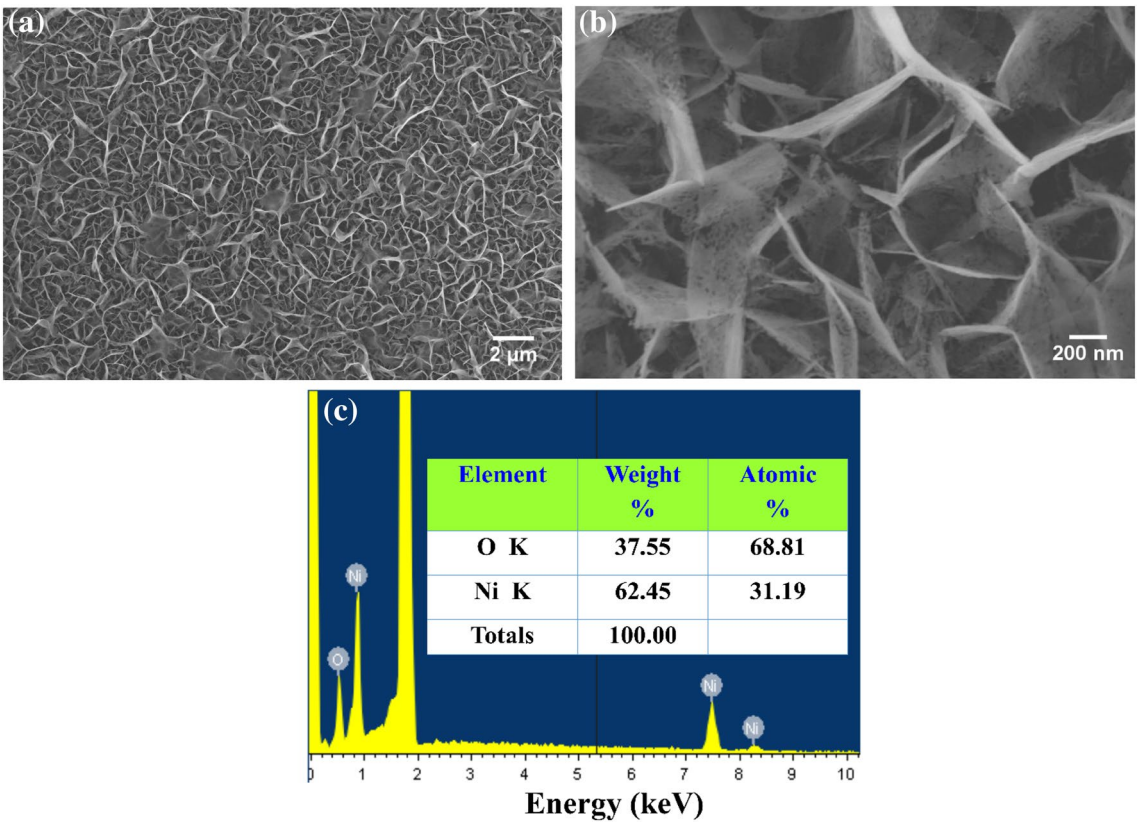

Fig. 2 FE-SEM micrographs of **a** low-magnification **b** high-magnification images of NiO NFs architecture on the Si substrate **c** EDX spectrum of NiO NFs architectures and its composition profile as the inset

of 3.045 MeV He^{++} particles and is shown in Fig. 3. The experimental RRBS data was simulated using the SIMNRA program [23]. The symbols in the RRBS spectrum represent the experimental data, whereas the solid traces corresponds to its best simulations. The backscattered signals of the elements such as Ni, O as well as Si substrate are clearly seen in the RRBS spectrum. Besides, the RRBS spectrum of *p*-NiO NFs/*n*-Si heterojunction shows the well distinct Si and Ni peaks, which implies that Ni does not diffused into the Si substrate. The thickness of NiO NFs architecture on the Si substrate estimated from the RRBS spectra is found to be ~400 nm.

Figure 4 presents the GIXRD pattern of *p*-NiO NFs/*n*-Si heterojunction architecture. The diffraction peaks centered at about the 2θ values of 37.6°, 43.8°, 63.4°, 76.2° and 80.2° corresponds to the reflection from the (111), (200), (220), (311) and (222) planes of face centered cubic phase of NiO and are found to be agree with the reported values [24, 25]. The diffraction pattern observed in the XRD spectra was indexed according to the standard JCPDS Card #47-1049. Besides the diffraction pattern of NiO, the broad peak centered at 2θ values of ~56°, corresponds to the reflection from the (311) plane of the Si substrate. No diffraction peaks other than NiO and the Si substrate were detected, suggesting high purity of the grown nanostructure. Our XRD result is in concurrence with the elemental analyses performed using EDX and RRBS measurements.

Raman spectroscopy is a powerful tool to the study the crystalline structure, structural disorder and defects in the nanostructured materials [26]. Raman spectra of *p*-NiO NFs/*n*-Si heterojunction excited using 532 nm laser line is shown in Fig. 5. The strong peak centered about 521 and 980 cm^{-1} are ascribed to the Si substrate peak, and found to be in good agreement with the previous reports [27]. It is reported that Raman peaks below 1200 cm^{-1} are originates

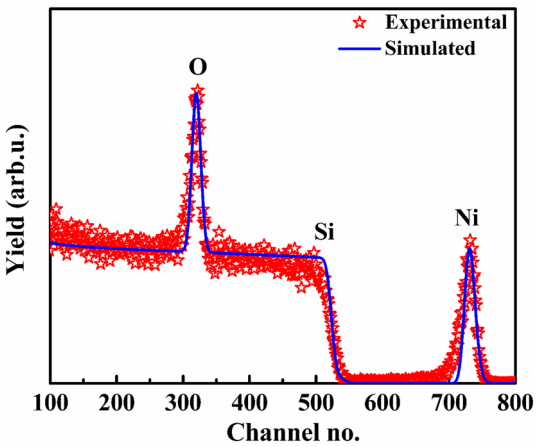

Fig. 3 Resonant Rutherford backscattering spectra of *p*-NiO NFs/*n*-Si heterojunction recorded using 3.045 MeV He^{++} particles

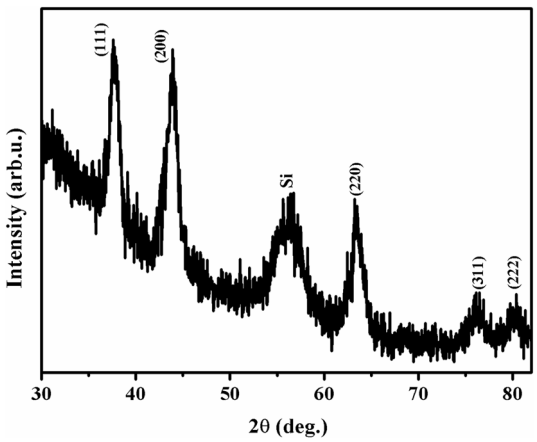

Fig. 4 GIXRD pattern of *p*-NiO NFs/*n*-Si heterojunction

from the first and second-order Raman scattering by the phonons in NiO, whereas the peaks above 1200 cm^{-1} are originates from the scattering by two-magnons (2M) in NiO [28]. The *p*-NiO NFs/*n*-Si heterojunction exhibits phonons scattering modes about 469 cm^{-1}, 508 cm^{-1}1, 568 cm^{-1}, 1162 cm^{-1}, 1396 cm^{-1}, and 1562 cm^{-1}, respectively. The intense peak centered at ~469 cm^{-1} originates from the disorder induced one-phonon (1P) scattering transverse optical (TO) mode. Raman peak centered about 508 cm^{-1} is induced by the strong phonon-magnon interaction at the surfaces of the NiO NFs architecture, so called one-phonon plus one-magnon (1P + 1M) interactions, which reveals the surface defects present in the NiO nanostructure [29]. Raman peaks at about 568 cm^{-1} and 1162 cm^{-1} are ascribed to the first and second-order longitudinal optical (LO) vibration modes of cubic NiO nanostructures, respectively, the peaks around 1396 and 1562 cm^{-1} correspond to the two-magnon

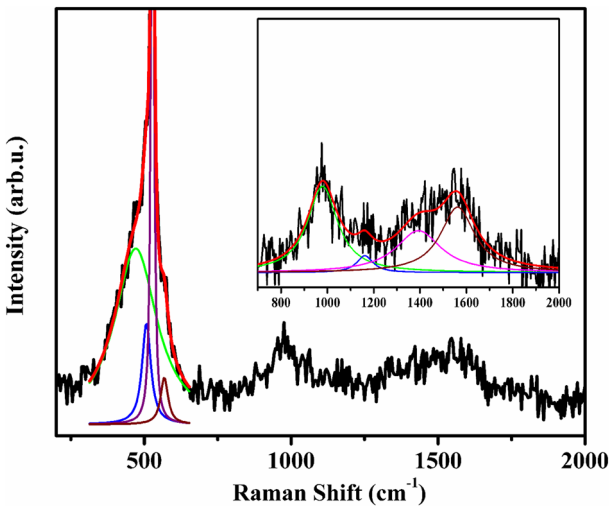

Fig. 5 Raman spectra of *p*-NiO NFs/*n*-Si heterojunction

(2M) scattering mode, which is mainly associated with Ni^{2+}–O_2–Ni^{2+} super-exchange interaction [30, 31]. According to the group theory analysis, the first-order Raman mode is originated from symmetry-breaking due to the presence of defects in the crystal lattice. It is evident that 1 LO and 2 LO phonon modes in NiO NFs architecture on the Si substrate has originated from the defects. To elucidate the defects present in the grown NiO architecture, photoluminescence (PL) measurement has been performed and presented in the subsequent section.

PL spectrum of NiO NFs architecture recorded using 355 nm laser excitation is shown in Fig. 6. In general, in metal oxide nanostructures, PL emission is broadly divided into two regions: (i) UV/near band-edge emission is influenced by the stoichiometric arrangement of cations and anions, and (ii) visible emission related to the intrinsic defects such as Ni interstitials (Ni_i), oxygen vacancies (Vo), oxygen interstitials (Oi), and oxygen antisite (O_{Ni}) respectively, present in the nanostructures, which are serves as the trapping centers for the electrons [32, 33]. Adler and Feinleib et al. have reported a series of absorption peaks below **− 4** eV for the NiO nanostructure and are ascribed to the transition involving $3d^8$-electrons of Ni^{2+} ions [34]. In the present study, emission bands are observed about ~ 413 nm (~ 3 eV), 435 nm (2.85 eV), 462 nm (2.68 eV) and 486 nm (2.55 eV), in addition with the Raman modes at 362, 370 and 376 nm. The observed Raman modes in the PL spectrum correspond to 1 LO, 2 LO and 2M phonon modes of NiO. It is reported that vacancies/interstitials on the cation sublattice are the primary defects in NiO and is known to be a metal-deficient compound [35, 36]. The cation defects in NiO nanostructure forms the energy levels below the conduction band-edge and the transition between the cation defects in NiO to the valance band gives rise the visible emission.

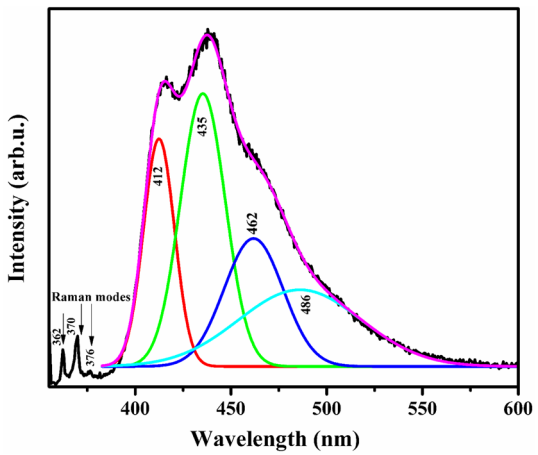

Fig. 6 Room temperature photoluminescence spectra of *p*-NiO NFs/*n*-Si heterojunction

The emission bands centered at 413 nm, corresponds to the violet emission, which is ascribed to the transition of trapped electrons at Ni interstitial (Ni_i) energy level to the valence band, blue emissions centered at 435 nm and 462 nm are ascribed to the transition of trapped electrons in singly ionized (V'_{Ni}), and doubly ionized (V''_{Ni}) nickel vacancies to the valence band, respectively. The green emission centered ~ 486 nm is ascribed to the oxygen vacancies. The observed emission bands are found to be consistent with the earlier reports [32, 37–40]. In the present study, the strong visible emission observed in the blue region reveals the presence of cationic defects and are found to be dominant in the grown NiO NFs architecture. The strong blue emission from the *p*-NiO NFs/*n*-Si heterojunction architecture reveals that the grown nanostructure can be used as the potential candidate for the blue light detection.

The schematic diagram of fabricated *p*-NiO NFs/*n*-Si heterojunction photodetector is shown in Fig. 7a. The I-V characteristics of *p*-NiO NFs/*n*-Si heterojunction photodetector recorded using blue light source (LED) of power 2.5 mW is shown in Fig. 7b. It is seen that *p*-NiO NFs/*n*-Si heterostructure exhibits good rectifying behavior in the dark, which implies *p*-*n* junction is formed at the interface of the *p*-NiO NFs and the *n*-Si substrate. The device shows the enhanced photocurrent under the blue light illumination. Under the illumination, *p*-NiO NFs/*n*-Si heterojunction exhibits very low leakage current of 3.3×10^{-8} A, and a large rectification ratio of ~ 366 at the reverse bias voltage of 3 V. It is observed that the photocurrent of *p*-NiO NFs/*n*-Si heterojunction is about 227 times higher than the corresponding dark current at an applied bias of − 3 V.

To choose the appropriate bias voltage for the transient measurements, voltage dependent sensitivity of the photodetector was performed from − 5 to + 5 V and is presented in Fig. 7c. The sensitivity (S) of the photodetector is estimated using the following formula [41]:

$$S = \frac{I_{ph} - I_{dark}}{I_{dark}} \quad ([1])$$

where, I_{ph} is photocurrent, and I_{dark} is dark current. The voltage-dependent sensitivity of the photodetector implies that *p*-NiO NFs/*n*-Si heterojunction is effectively working in reverse bias and exhibits maximum sensitivity of 227 at − 3 V. To illustrate the mechanism of photoresponse characteristics of reverse biased *p*-NiO NFs/*n*-Si heterojunction photodetector, the energy-band diagram of *p*-NiO NFs/*n*-Si heterojunction under illumination with blue light is presented in Fig. 7d. At the interface, *p*-NiO exhibits the downward band-bending and the *n*-Si shows the upward band-bending due to the different conduction (E_C) and the valence band (E_V) energy levels of *p*-NiO and *n*-Si.

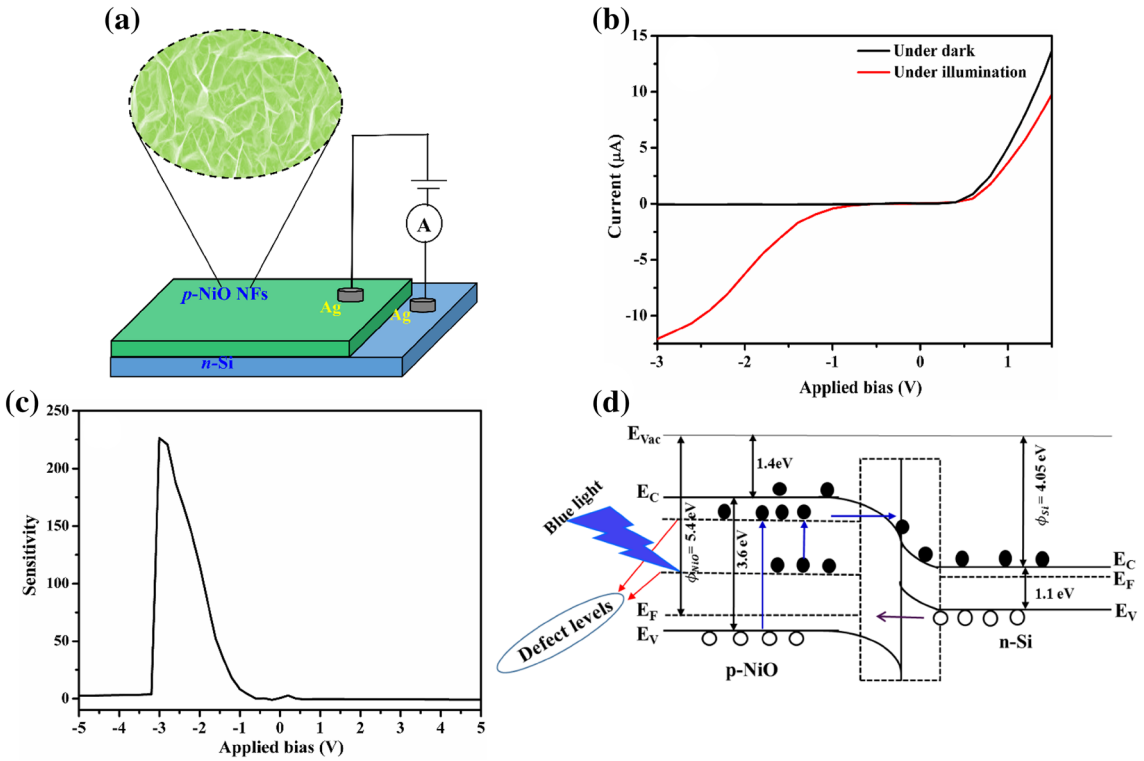

Fig. 7 **a** The fabricated *p*-NiO NFs/*n*-Si heterojunction photodetector, **b** I–V characteristics of the *p*-NiO NFs/*n*-Si heterojunction photodetector in the dark (black) and under illumination (red) from blue light of power 2.5 mW and an applied bias ranging from −3 V to +1.5 V, **c** Voltage-dependent sensitivity of the photodetector as a function of applied voltage, **d** The schematic energy band diagram of reverse biased *p*-NiO/*n*-Si heterojunction

Under the blue light illumination, the electron–hole pairs are generated in the *p*-NiO NFs/*n*-Si heterojunction. In the meantime, the applied reverse-bias build the electric field at the interface serves as an electromotive force which drives the electrons to the underlying *n*-type Si substrate as well as holes to the *p*-type NiO NFs.

Figure 8 presents time-dependent photoresponse switching behavior of *p*-NiO/*n*-Si heterojunction photodetector for the applied bias ranging from −1 to −3 V in the dark and under the illumination of blue LED of radiation of 450 nm and power of 2.5 mW. The time-dependent photoreponse measurement of the device with ON/OFF switching time period of 60 s/ 20 s exhibits almost equal photocurrent for all the ON/OFF states, which reveals better stability and repeatability of the device. It is observed that under the reverse bias of 1 V, the device exhibits lower photocurrent. On further increasing the applied reverse bias from 1 V to 3 V, the device exhibits enhanced photocurrent. The lower photocurrent at low-bias voltage is ascribed to the surface defect states that existing in the NiO NFs architecture capture photogenerated electrons. The increased applied reverse bias broaden the depletion region and built-in electric field at the interface leading the effective separation of charge carriers, resulting the large concentration of free electrons driven to the underlying *n*-type Si substrate contributing to the higher photocurrent. The presence of surface defects in NiO NFs architecture is well evidenced from the PL spectra. From Fig. 8a, it is found that under the reverse bias, the photocurrent of the device increases slowly and reaches the saturation, and then return to its initial level shortly after the illumination is turned o. The photoresponse speed of the device is estimated by the parameters: the response time (τ_r), the time required to increase the photocurrent from 10 to 90% of its peak value and recovery time (τ_d), is the time required to fall down the current from 90 to 10% of its maximum value [42, 43], and are illustrated in Fig. 8b, c. The response time (τ_r) and recovery time (τ_d) of the device is found to be ~6.18 s and ~1.83 s. The observed high photoresponse time and the fast recovery time of the device is described as follows: during the illumination, i.e. the device switching over from OFF to ON state, the device required time to transport the photogenerated charge carriers due to the slow release of trapped photogenerated carriers by the surface defects states, while the device switching over from ON to OFF state, *p*–*n* heterojunction begins to deplete further, which in turn promote fast carrier recombinations resulting decreased recovery time. The higher photoresponse observed at the reverse bias of 3 V is ascribed to the strong

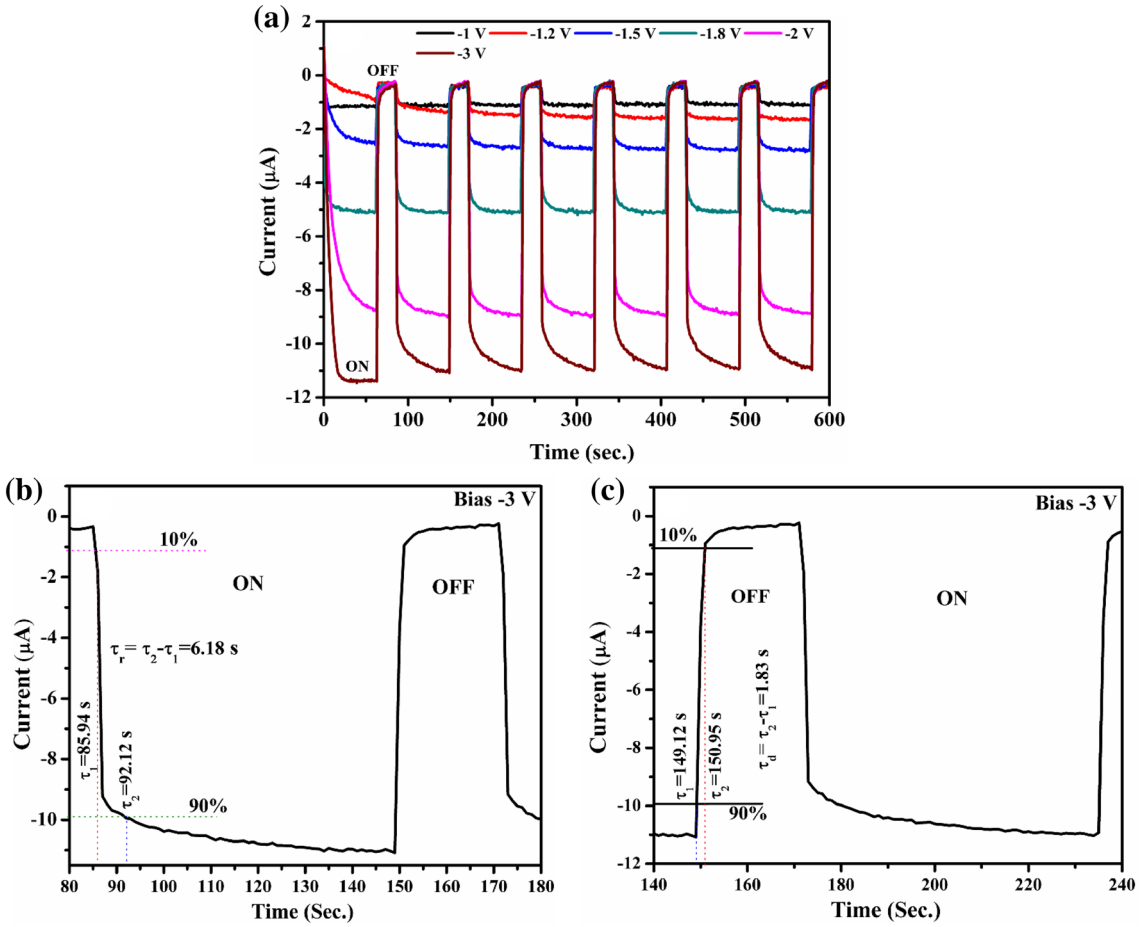

Fig. 8 **a** switching response of *p*-NiO NFs/*n*-Si heterojunction illuminated by the blue light of power 2.5 mW with applied reverse bias of voltages ranging between −1 V and −3 V. **b, c** reveals the magnified rising and falling edge of the photoresposne curve at the fixed bias of −3 V, where, τ_r is the time interval for the rise of photoresponse curve from 10 to 90% and τ_d is the time interval for the decay of the photoresponse curve from 90 to 10% of its maximum value

electric field built at the interface prevents the formation electron–hole pairs, thus, favoring the transport of photogenerated electrons to the underlying Si substrate. The observed response and the recovery time of *p*-NiO/*n*-Si heterojunction photodetector is found to be efficient in comparison with the earlier reports dealing with the metal oxides based photodetectors [12, 20, 42, 44–47], and are presented in Table 1. The enhanced photocurrent at the reverse bias of 3 V is ascribed

Table 1 The comparison of the characteristics parameters of metal-oxides based heterojunction photodetectors obtained from the literature with the present work

Materials	Wavelength used/ detection range (nm)	Type of bias/ bias voltage (V)	Rise/Fall time (s)	Leakage current (A)	Reference
p-NiO/n-Si		reverse bias/−3	6.18/1.83	3.3×10^{-8}	present work
p-NiO/p-Si	385, 515, & 620	reverse bias/ −1	0.5 / 0.526	3.91×10^{-8}	[12]
p-NiO/n-Si(111)	350–600	reverse bias/−2	< 30 ms	–	[20]
NiO/TiO_2 NRs	365	reverse bias/0 and − 1	38.5/4.2 & 28.9/2.0	–	[42]
rGO/Si	382	reverse bias/ −2	–	2.12×10^{-6}	[44]
p-Si/n-ZnO NRs	360	reverse bias/ −4	11/14	–	[45]
TiO_2/NiO	350	self-powered	1.2/7.1	–	[46]
p-NiO/n-ZnO	365	reverse bias/ −3.5	6.4/11.3	–	[47]

to the photogenerated electrons in NiO NFs driven to the underlying Si substrate and holes to the NiO NFs under the external electric field built at the interface.

4 Conclusion

In this work, the *p*-NiO/*n*-Si heterojunction photodetector was fabricated and its photoresponse characteristics were studied. GIXRD measurements reveal the grown NiO NFs architecture is face centered cubic phase of NiO. The I–V characteristics of the photodetector shows good rectifying behavior in the reverse bias and the voltage-dependent sensitivity measurements manifest the device has maximum sensitivity at − 3 V under blue light illumination. The time-dependent photoresponse behavior reveals the fabricated device exhibits good stability and repeatability and its photoresponse and recovery time are found to be 6.18 s and 1.83 s, respectively. The origin of the photoresponse behavior of device is attributed to the strong built-in electric field at the interface driven the electrons to the *n*-Si and holes to the *p*-NiO. Our experimental investigations manifested that the fabricated *p*-NiO/*n*-Si heterojunction photodetector is a promising candidate for high speed, high sensitive, low voltage, and large current photodetection applications.

Acknowledgements One of the authors, G. J wishes to thank the Science and Engineering Research Board (SERB), Govt. of India, for financial support through Fast-Track Young Scientist Scheme (Grant No. YSS/2015/000240).

References

1. Y. An, A. Behnam, E. Pop, A. Ural, Metal-semiconductor-metal photodetectors based on graphene/p-type silicon Schottky junctions. Appl. Phys. Lett. **102**, 013110 (2013)
2. D. Zheng, H. Fang, M. Long, F. Wu, P. Wang, F. Gong, X. Wu, J.C. Ho, L. Liao, W. Hu, High-performance near-infrared photodetectors based on p-type SnX (X = S, Se) nanowires grown *via* chemical vapor deposition. ACS Nano **12**(7), 7239–7245 (2018)
3. G. Jayalakshmi, K. Saravanan, B.K. Panigrahi, B. Sundaravel, M. Gupta, Tunable electronic, electrical and optical properties of graphene oxide sheets by ion Irradiation. Nanotechnology **29**, 185701 (2018)
4. K. Saravanan, G. Jayalakshmi, R. Krishnan, B. Sundaravel, B.K. Panigrahi, Influence of C or In buffer layer on photoluminescence behaviour of ultrathin ZnO film. J. Appl. Phys. **120**, 095302 (2016)
5. G. Jayalakshmi, K. Saravanan, T. Balasubramanian, Influence of oxygen pressure on structural, optical and magnetic properties of pure ZnO films. J. Mater. Sci **25**, 2024 (2014)
6. H.Y. Chen, K.W. Liu, X. Chen, Z.Z. Zhang, M.M. Fan, M.M. Jiang, X.H. Xie, H.F. Zhao, D.Z. Shen, Realization of self-powered ZnO MSM UV photodetector with high responsivity using asymmetric pair of Au electrodes. J. Mater. Chem. C **2**, 9689 (2014)
7. G. Rajan, A. Kaur, H.K. Paliwal, V. Yadav, Gupta, M. Tomar, Plasmonic assisted enhanced photoresponse of metal nanoparticle loaded ZnO thin film ultraviolet photodetectors. J. Phys. D **47**, 425102 (2014)
8. L. Wang, W. Yang, H. Chong, L. Wang, F. Gao, L. Tian, Z. Yang, Efficient ultraviolet photodetectors based on TiO_2 nanotube arrays with tailored structures. RSC Adv. **5**, 52388 (2015)
9. S. Gundimeda, N. Krishna, A. Aggarwal, N.D. Sharma, K.K. Sharma, S. Maurya, Husale, G. Gupta, Fabrication of non-polar GaN based highly responsive and fast UV photodetector. Appl. Phys. Lett. **110**, 103507 (2017)
10. E. Aldalbahi, M. Li, Rivera, R.Velazquez, T., X. Altalhi, Peng, P.X. Feng, A new approach for fabrications of SiC based photodetectors. Sci. Rep. **6**, 23457 (2016)
11. X. Chang, Y.F. Wang, X. Zhang, Z. Liu, J. Fu, S. Fan, R. Bu, J. Zhang, W. Wang, H.X. Wang, J. Wang, UV-photodetector based on NiO/diamond film. Appl. Phys. Lett. **112**, 032103 (2018)
12. S. Parida, M. Kim, S. Oh, M. Jung, J.H. Baek, H. Ryou, Kim, Nanostructured-NiO/Si heterojunction photodetector. Mater. Sci. Semicond. Process. **71**, 29–34 (2017)
13. R.K. Gupta, A.A. Hendi, M. Cavas, A.A. Al-Ghamdi, O.A. Al-Hartomy, R.H. Aloraini, F. El-Tantawy, F. Yakuphanoglu, Improvement of photoresponse properties of NiO/p-Si photodiodes by copper dopant. Physica E **56**, 288 (2014)
14. G. Jayalakshmi, K. Saravanan, B.K. Panigrahi, P. Magudapathy, High efficient electron field emission from rGO conformally coated NiO nanoflakes architecture. J. Mater. Sci. **29**, 14689 (2018)
15. J.M. Choi, S. Im, Ultraviolet enhanced Si-photodetector using p-NiO films. Appl. Surf. Sci. **244**, 435–438 (2005)
16. L. Duan, P. Wang, W. Zhang, X. Yu, J. Fan, F. Wei, ZnO homojunction ultraviolet photodetector based on p-type dual-doped film and n-type nanorods. Chem. Phys. Lett. **618**, 123 (2015)
17. Y. Luo, B. Yin, H. Zhang, Y. Qiu, J. Lei, Y. Chang, Y. Zhao, J. Ji, L. Hu, Fabrication of p-NiO/n-ZnO heterojunction devices for ultraviolet photodetectors via thermal oxidation and hydrothermal growth Processes. J. Mater. Sci. **27**, 2342–2348 (2016)
18. R. Debnath, T. Xie, B. Wen, W. Li, J.Y. Ha, N.F. Sullivan, N.V. Nguyen, A. Motayed, A solution-processed high-efficiency p-NiO/n-ZnO heterojunction photodetector. RSC Adv. **5**, 14646 (2015)
19. A. Ahmed, M. Devarajan, N. Afza, Fabrication and characterization of high performance MSM UV photodetector based on NiO film. Sens. Actuator A-Phys. **262**, 78 (2017)
20. Y. Zhang, T. Ji, W. Zhang, G. Guan, Q. Ren, K. Xu, X. Huang, R. Zou, J. Hu, A self-powered broadband photodetector based on an n-Si(111)/p-NiO heterojunction with high photosensitivity and enhanced external quantum efficiency. J. Mater. Chem. C **5**, 12520 (2017)
21. D. Zhang, S. Nozaki, K. Uchida, NiO/Si heterostructures formed by UV oxidation of Nickel deposited on Si substrates. J. Vac. Sci. Technol. B **32**, 031202 (2014)
22. C. Gandhi, S.Y. Wu, Strong deep-level-emission photoluminescence in NiO nanoparticles. Nanomaterials **7**, 231 (2012)
23. M. Mayer, S.I.M.N.R.A. User's, Guide, Report IPP 9/113 (Max-Planck-Institutfur Plasmaphysik, Garching, 1997)
24. H. Yan, D. Zhang, J. Xu, Y. Lu, Y. Liu, K. Qiu, Y. Zhang, Y. Luo, Solution growth of NiO nanosheets supported on Ni foam as high-performance electrodes for supercapacitors. Nanoscale Res. Lett. **9**, 424 (2014)
25. B. Subramanian, M. Mohamed Ibrahim, V. Senthilkumar, K.R. Murali, V.S. Vidhya, C. Sanjeeviraja, M. Jayachandran, Optoelectronic and electrochemical properties of nickel oxide (NiO) films deposited by DC reactive magnetron sputtering. Physics B **403**, 4104–4110 (2008)

26. G. Jayalakshmi, K. Saravanan, S. Balakumar, T. Balasubramanian, Swift heavy ion induced modifications in structural, optical & magnetic properties of pure and V doped ZnO films. Vacuum **95**, 66–70 (2013)
27. K. Uchinokura, T. Sekine, E. Matsuura, Raman scattering by silicon. Solid State Commun. **11**, 47 (1972)
28. P. Ravikumar, D. Taparia, P. Alagarsamy, Thickness-dependent thermal oxidation of Ni into NiO thin films. J. Supercond. Nov. Magn. (2018). https://doi.org/10.1007/s10948-018-4651-6
29. N. Mironova-Ulmane, A. Kuzmin, J. Grabis, I. Sildos, V.I. Voronin, I.F. Berger, V.A. Kazantsev, Structural and magnetic properties of nickel oxide nanopowders. Solid State Phenomena **168–169**, 341–344 (2011)
30. W.J. Duan, S.H. Lu, Z.L. Wu, Y.S. Wang, Size effects on properties of NiO nanoparticles grown in alkali salts. J. Phys. Chem. C **116**, 26043–26051 (2012)
31. K. Varunkumar, R. Hussain, G. Hegde, A.S. Ethiraj, Effect of calcination temperature on Cu doped NiO nanoparticles prepared via wet-chemical method: Structural, optical and morphological studies. Mater. Sci. Semicond. Process. **66**, 149 (2017)
32. S. Majumder, S. Bhattacharjee, C.K. Ghosh, NiO/Ag heterostructure: enhanced UV emission intensity, exchange interaction and photocatalytic activity. RSC Adv. **6**, 56503–56510 (2016)
33. G. Jayalakshmi, K. Saravanan, J. Pradhan, P. Magudapathy, B.K. Panigrahi, Facile synthesis and enhanced luminescence behavior of ZnO: reduced graphene oxide(rGO) hybrid nanostructure. J. Lumin. **203**, 1–6 (2018)
34. Adler, J. Feinleib, Electrical and optical properties of narrow-band materials. Phys. Rev. B **2**, 3112–3134 (1970)
35. N.L. Peterson, C.L. Wiley, Point defects and diffusion in NiO. J. Phys. Chem. Solids **46**, 43 (1985)
36. C. Diaz-Guerra, A. Remon, J.A. Garcia, J. Piqueras, Cathodoluminescence and photoluminescence spectroscopy of NiO. Phys. Stat. Sol. (a) **163**, 497 (1997)
37. K.N. Patel, M.P. Deshpande, K. Chauhan, P. Rajput, V. Sathe, S. Pandya, Synthesis, structural and photoluminescence properties of nanocrystalline Cu doped NiO. Mater. Res. Express (2018) https://doi.org/10.1088/2053-1591/aa90ad
38. M. Patel, H.S. Kim, J. Kim, All transparent metal oxide ultraviolet photodetector. Adv. Electron. Mater. **1**, 1500232 (2015)
39. P.A. Sheena, K.P. Priyanka, N. Aloysius Sabu, S. Ganesh, T. Varghese, Effect of electron beam irradiation on the structure and optical properties of nickel oxide nanocubes. Bull. Mater. Sci. **38**, 825–830 (2015)
40. S.M. Meybodi, S.A. Hosseini, M. Rezaee, S.K. Sadrnezhaad, D. Mohammadyani, Synthesis of wide band gap nancrystalline NiO powder via sonochemical method. Ultrason. Sonochem. **19**, 841 (2012)
41. Y. Wan, S. Gao, L. Li, J. Zhang, H. Fan, S. Jiao, J. Wang, Q. Yu, D. Wang, Efficient UV photodetector based on heterojunction of n-ZnO nanorods/p-diamond film. J. Mater. Sci (2017) https://doi.org/10.1007/s10854-017-6904-8
42. Y. Gao, J. Xu, S. Shi, H. Dong, Y. Cheng, C. Wei, X. Zhang, S. Yin, L. Li, TiO_2 nanorod arrays based self-powered UV photodetector: heterojunction with NiO nanoflakes and enhanced UV photoresponse. ACS Appl. Mater. Interfaces **10**(13), 11269–11279 (2018)
43. B.D. Boruah, A. Misra, Effect of magnetic field on photoresponse of cobalt integrated zinc oxide nanorods. ACS Appl. Mater. Interfaces **8**(7), 4771–4780 (2016)
44. T. Chandrakalavathi, K.R. Peta, R. Jeyalakshmi, Enhanced UV photoresponse with Au nanoparticles incorporated rGO/Si heterostructure. Mater. Res. Express **5**, 025011 (2018)
45. N.H. Al-Hardan, A. Jalar, M.A. Abdul Hamid, L.K. Keng, N.M. Ahmed, R. Shamsudin, A wide-band UV photodiode based on n-ZnO/p-Si heterojunctions. Sens Actuat A **207**, 61–66 (2014)
46. L. Zheng, F. Teng, Z. Zhang, B. Zhao, X. Fang, Large scale, highly efficient and self-powered UV photodetectors enabled by all-solid-state n-TiO_2 nanowell/p-NiO mesoporous nanosheet heterojunctions. J. Mater. Chem. C **4**, 10032 (2016)
47. W. Dai, X. Pan, S. Chen, C. Chen, Z. Wen, H. Zhang, Z. Ye, Honeycomb-like NiO/ZnO heterostructured nanorods: photochemical synthesis,characterization, and enhanced UV detection performance. J. Mater. Chem. C **2**, 4606 (2014)